RSC Advances

PAPER

View Article Online
View Journal | View Issue

Cite this: *RSC Adv.*, 2021, **11**, 36682

Theoretical prediction of structural, mechanical, and electronic properties of Janus $GeSnX_2$ (X = S, Se, Te) single-layers

Khang D. Pham *

Received 22nd October 2021
Accepted 3rd November 2021

DOI: 10.1039/d1ra07813e

rsc.li/rsc-advances

The breaking of the vertical mirror symmetry in two-dimensional Janus structures has given rise to many outstanding features that do not exist in the original materials. In this work, we study the structural, mechanical, and electronic properties of Janus $GeSnX_2$ (X = S, Se, Te) single-layers using density functional theory. The stability of the investigated Janus structures has been tested through the analysis of their phonon dispersions and elastic parameters. It is found that, with low in-plane stiffness, Janus $GeSnX_2$ single-layers are more mechanically flexible than other two-dimensional materials and their mechanical properties exhibit very high anisotropy. All three single-layers are semiconductors and their bandgap can be altered easily by strain engineering. Due to the asymmetric structure, a vacuum level difference between the two sides is observed, leading to the difference in work function on the two sides of single-layers. Our findings not only provide necessary information about the physical properties of Janus $GeSnX_2$ single-layers but also provide the impetus for further studies on these interesting materials both theoretically and experimentally.

1 Introduction

Two-dimensional (2D) layered nanomaterials have been one of the objects that have attracted much attention from the scientific community over the past two decades because of their outstanding physical properties and potential applications in nanotechnology.[1–4] The discovery of graphene in 2004 (ref. 5) opened a new era in the study of 2D systems both theoretically and experimentally. Immediately after that, many new graphene-like structures have been experimentally reported, such as silicene,[6] germanene,[7] stanene,[8] transition metal dichalcogenides (TMDs),[9] monochalcogenides,[10–12] and so on. In parallel with experimental studies, theoretical studies have systematically investigated 2D layered nanomaterials with many different methods[13–15] and have obtained many positive achievements.[16–19] Among them, 2D metal monochalcogenide structures emerge as very promising materials with many applications in various fields of electronic and optoelectronic nanotechnology.[4,20]

The group IV monochalcogenide single-layers, such as SnS, GeS, or GeSe, are narrow gap semiconductors with the orthorhombic layered crystal structure.[21,22] Similar to other 2D materials, the group IV monochalcogenides possess strong covalent bonding in each single-layer but the layers are held together only by weak van der Waals forces. Besides, they have moderate cohesive energies,[23] which support for isolation of these single-layers by mechanical or liquid-phase exfoliation. Fei and co-workers have indicated that the group IV monochalcogenides exhibit giant piezoelectricity and they can be promising candidates for applications in piezotronics.[24]

In 2017, the asymmetric Janus MoSSe was surprisingly successfully fabricated experimentally.[25,26] The creation of asymmetric Janus structures from existing symmetric materials has opened up a new approach in the study of 2D layered materials. A series of Janus based on 2D structures have been investigated, from Janus dichalcogenides[27,28] to Janus monochalcogenides.[29–32] Along with that trend, Janus group IV chalcogenides, such as Ge_2SSe, Sn_2SeTe[33] or GeSSe and SnSSe[34] has also been studied very recently. It was found that many new physical properties were found in Janus structures due to the breaking of the mirror symmetry structure.[30,34] In addition, the vertical asymmetry in the Janus structure also gave rise to an intrinsic built-in electric field, which leads to difference in the vacuum levels between the two sides of the Janus monolayers.[31,35] In this study, we deal with the structural, mechanical, and electronic properties of Janus $GeSnX_2$ (X = S, Se, Te) single-layers by mean of density functional theory (DFT). Obtained results reveal that all three Janus structures of $GeSnX_2$ are stable and can be synthesized as free-standing single-layers. The main content of this work is to focus on the mechanical and electronic properties of the $GeSnX_2$ single-layers. The influence of mechanical strain on the electronic characteristics is also systematically investigated in this work.

Institute of Applied Technology, Thu Dau Mot University, Binh Duong Province 75000, Vietnam. E-mail: phamdinhkhang@tdmu.edu.vn

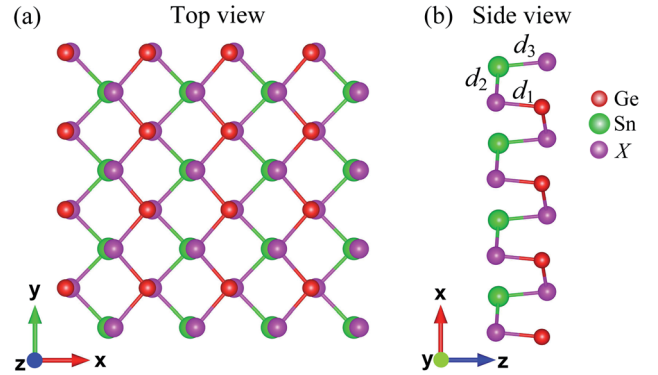

Fig. 1 Top (a) and side (b) views of atomic structure of Janus $GeSnX_2$ (X = S, Se, Te). Ge, Sn, and X atoms are indicated by red, green, and purple balls, respectively.

2 Computational details

All calculations in the present work are fulfilled within the density functional theory (DFT) as implemented in the Quantum Espresso code.[36] The projector augmented wave potentials are used to investigate the interactions between the valence electrons and the core.[37] The Perdew–Burke–Ernzerhof (PBE) functional in the generalized gradient approximation is used to consider the exchange–correlation interactions. We also use the Heyd–Scuseria–Ernzerhof functional (HSE06) to correct the band structures of the Janus single-layers.[38] The Grimme's DFT-D2 method[39] is used to consider the long-range weak van der Waals interactions in the layered materials. The energy cutoff of 500 eV is selected for the plane waves and the criterion for force-convergence is to be 10^{-3} eV $Å^{-1}$. To reduce the interactions between neighbor slabs, we insert the vacuum space of 20 Å along the vertical direction. 15 × 15 × 1 *k*-point meshes are built *via* the Monkhorst–Pack scheme[40] for the optimization process and calculations of the electronic properties. Vibrational properties of the investigated Janus structures are calculated by the density-functional perturbation theory (DFPT)[41] through the Quantum Espresso package.[36] The elastic constants are evaluated from the energy change by applying small strains ranging from −1% to +1% with steps of 0.5% and the total energy per unit area is evaluated on a 10 × 10 × 1 grid.

3 Results and discussion

3.1 Atomic structure and stability

The atomic structure of Janus $GeSnX_2$ (X = S, Se, Te) single-layers is presented in Fig. 1. The lattice constants *a* and *b* for all materials are summarized in Table 1. It is found that the lattice constants *a* and *b* (along the *x* and *y* axes, respectively) increase with an increase in the size of the X element, from S to Te. For each single-layer, the lattice *a* is larger than *b*. That is similar to the other orthorhombic structure in that the lattice parameter along the *x*-axis (armchair direction) is longer than that along the *y*-axis.[42] As shown in Table 1, Janus $GeSnX_2$ has a low directional anisotropic structure that is comparable with the group IV monochalcogenides.[23,42] The anisotropy parameter *a*/*b* varies from 1.15 to 1.05. The lighter the material, the larger the anisotropy parameter *a*/*b* is. The bond lengths Gn–X and Sn–X follow a similar trend for the lattice constants that these bond lengths increase as element X changes from S to Te. Calculated the bond lengths and bond angles of $GeSnX_2$ are also presented in Table 1.

To test the strength of the covalent bond in the Janus $GeSnX_2$ structures, we calculate their cohesive energy E_{coh} as the following:

$$E_{coh} = \frac{N_{Ge}E_{Ge} + N_{Sn}E_{Sn} + N_X E_X - E_{tot}}{N_{Ge} + N_{Sn} + N_X}, \quad (1)$$

where E_{Ge}, E_{Sn}, and E_X indicate the single-atom energies of the elements Ge, Sn, and X, respectively, E_{tot} stands for the total energy of $GeSnX_2$ monolayer; and N_{Ge}, N_{Sn}, and N_X are the number atoms of the Ga, S, and X in the unit-cell. Our calculated results demonstrate that all three monolayers of $GeSnX_2$ are energetically favorable. The calculated results for the cohesive energy of $GeSnX_2$ monolayers are also presented in Table 1. The E_{coh} of $GeSnX_2$ is form 3.74 to 4.42 eV per atom, which is comparable with that of the group IV monochalcogenides.[43,44]

We next analyze the vibrational properties of the systems to evaluate their dynamical stability. The phonon dispersion bands of Janus $GeSnX_2$ are presented in Fig. 2. The unit cell of $GeSnX_2$ contains four atoms, including one Ge, one Sn, and two X atoms, therefore its phonon band consists of 12 vibrational modes. There are three acoustic vibrational modes in the low-frequency regime meanwhile nine optical are in higher frequency regimes. It is noted that, as shown in Fig. 2, the acoustic and optical vibrational modes coexist partially in the same frequency regime and no gap between acoustic and optical vibrational modes is observed in all three models of $GeSnX_2$. This may lead to robust optical-acoustic scattering in these materials and as a result, they will have low thermal conductivity. Most importantly, the phonon diagrams of all three structures contain only positive frequencies. There are no soft modes in their phonon spectrum. This suggests that all considered configurations are dynamically stable and that they can be experimentally synthesized as free-standing sheets.

Table 1 Lattice constants *a* and *b*, bond lengths $d_{1,2,3}$, bond angle ϕ, anisotropy parameter *a*/*b*, and cohesive energy E_{coh} of Janus $GeSnX_2$ (X = S, Se, Te) single-layers

	a (Å)	*b* (Å)	d_1 (Å)	d_2 (Å)	d_3 (Å)	$\phi_{\angle XSnX}$ (deg.)	$\phi_{\angle GeXSn}$ (deg.)	*a*/*b*	E_{coh} (eV)
$GeSnS_2$	4.42	3.86	2.41	2.68	2.60	90.37	105.09	1.15	4.42
$GeSnSe_2$	4.45	4.11	2.55	2.85	2.72	93.33	97.89	1.08	4.09
$GeSnTe_2$	4.60	4.38	2.76	3.05	2.91	97.20	91.22	1.05	3.74

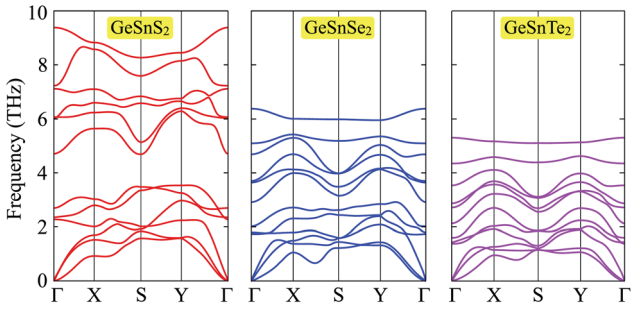

Fig. 2 Phonon spectra of Janus $GeSnX_2$ single-layers (X = S, Se, Te).

3.2 Mechanical properties

In this part, we analyze the mechanical properties of Janus $GeSeX_2$ based on the evaluations of their elastic constants C_{ij} (using Voigt notation). The C_{ij} constants are important parameters that can support the evaluation of elastic characteristics as well as mechanical properties of the materials. With the rectangular lattice, there are four independent constants, including C_{11}, C_{12}, C_{22}, and C_{66}. The calculated elastic constants C_{ij} of Janus $GeSnX_2$ single-layers are summarized in Table 2. It is found that all four C_{ij} constants are positive, implying that the Janus $GeSnX_2$ are mechanically stable under small in-plane deformations. Also, it can be seen that the C_{22} is larger than both C_{11} and C_{12}, suggesting that the materials have greater rigidity in the zigzag direction (y axis). There is high anisotropy in the elastic constants of the Janus $GeSnX_2$ single-layers. These mechanical characteristics of Janus GeSnX are similar to the group IV monochalcogenides.[24]

Unlike graphene or the group III monochalcogenides, the group IV monochalcogenides and also Janus group IV monochalcogenides have an anisotropic in-plane structure. Therefore, their in-plane stiffness is very sensitive to the investigated direction. The direction-dependent 2D Young's modulus $Y_{2D}(\varphi)$ and Poisson's ratio $\vartheta(\varphi)$ are given by[34]

$$Y_{2D}(\varphi) = \frac{C_{11}C_{22} - C_{12}^2}{C_{11}\Pi^4 + C_{22}\Lambda^4 + \Pi^2\Lambda^2\left(\frac{C_{11}C_{22} - C_{12}^2}{C_{66}} - 2C_{12}\right)}, \quad (2)$$

$$\vartheta(\varphi) = \frac{C_{12}(\Pi^4 + \Lambda^4) - \Pi^2\Lambda^2\left(C_{11} + C_{22} - \frac{C_{11}C_{22} - C_{12}^2}{C_{66}}\right)}{C_{11}\Pi^4 + C_{22}\Lambda^4 + \Pi^2\Lambda^2\left(\frac{C_{11}C_{22} - C_{12}^2}{C_{66}} - 2C_{12}\right)}, \quad (3)$$

where $\Pi = \sin\varphi$ and $\Lambda = \cos\varphi$ with φ is the polar angle relative to the x-axis (armchair direction).

Table 2 Four independent elastic constants C_{11}, C_{22}, C_{12}, and C_{66} of Janus $GeSnX_2$ single-layers

	C_{11} (N m^{-1})	C_{12} (N m^{-1})	C_{22} (N m^{-1})	C_{66} (N m^{-1})
$GeSnS_2$	14.78	17.58	38.68	17.27
$GeSnSe_2$	19.18	18.92	40.68	18.52
$GeSnTe_2$	22.15	16.25	41.03	20.99

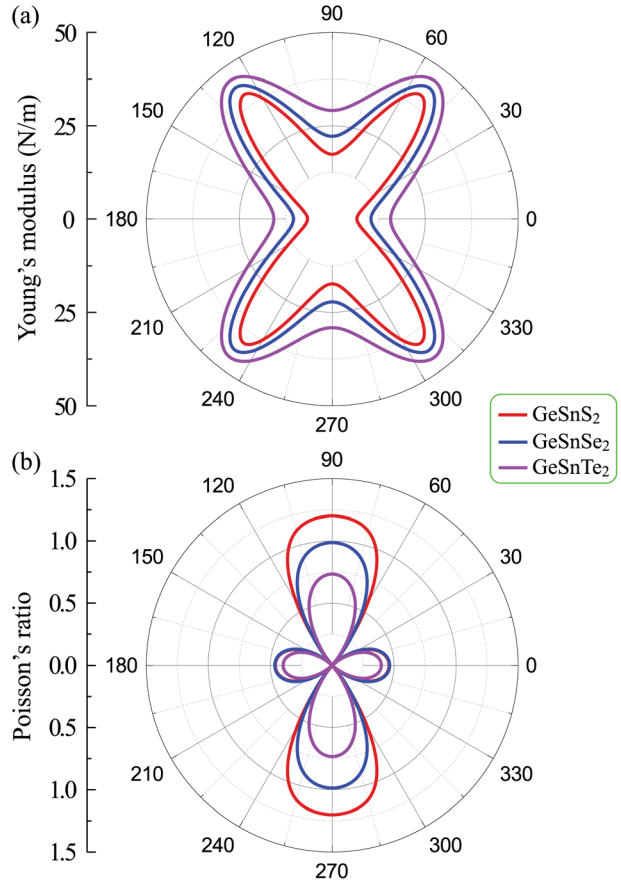

Fig. 3 Directional dependence of Young's modulus (a) and Poisson's ratio (b) of Janus $GeSnX_2$ single-layer.

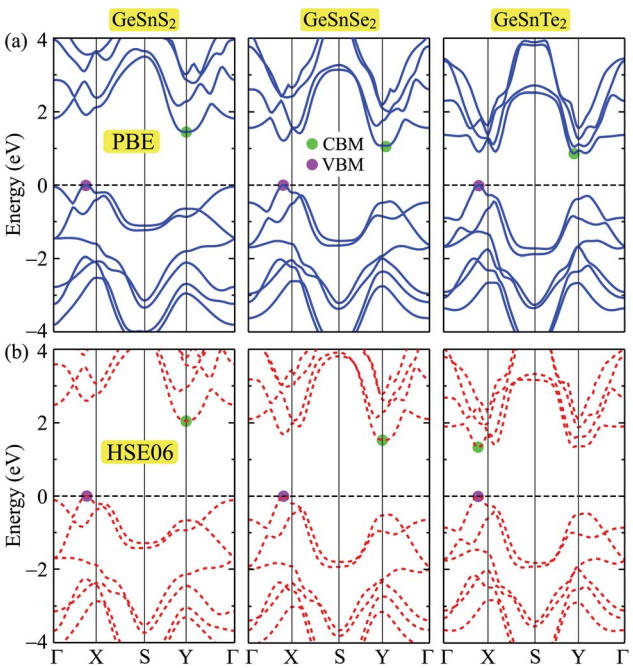

Fig. 4 Band structures of $GeSnS_2$, $GeSnSe_2$, and $GeSnTe_2$ single-layers at the PBE (a) and HSE06 (b) levels.

Table 3 Band gaps at the PBE and HSE06 levels, vacuum level difference $\Delta\Phi$, work functions on the XGe-side Φ_1 and SnX-side Φ_2 of Janus $GeSnX_2$ single-layers. All parameters are in units of eV

	E_g^{PBE}	E_g^{HSE06}	$\Delta\Phi$	Φ_1	Φ_2
$GeSnS_2$	1.45	2.05	0.46	4.79	5.25
$GeSnSe_2$	1.07	1.53	0.42	4.55	4.96
$GeSnTe_2$	0.87	1.33	0.31	4.46	4.77

From atomic structures, as shown in Fig. 1, we can qualitatively predict that the Janus $GeSnX_2$ is the softest along the armchair direction (the x axis). This prediction is consistent with calculated results as presented in Table 2. This prediction is supported by the polar diagrams of $Y_{2D}(\varphi)$ and $\vartheta(\varphi)$ in Fig. 3. It is demonstrated that the mechanical characteristics of $GeSnX_2$ are highly directional anisotropic. We can see that Y_{2D} along the armchair direction $Y_{2D}(0°)$ is the smallest. It is calculated that the $Y_{2D}(0°)$ for $GeSnS_2$, $GeSnSe_2$, and $GeSnTe_2$ single-layers is 6.63, 10.42, and 15.72 N m^{-1}, respectively. Meanwhile, the Young's modulus along the zigzag direction $Y_{2D}(90°)$ is higher than $Y_{2D}(0°)$. From Fig. 3(a), it can be seen that the $GeSnX_2$ is the hardest corresponding to about ±54° relative to the armchair direction. The maximum Y_{2D} for $GeSnS_2$, $GeSnSe_2$, and $GeSnTe_2$ is 40.86, 43.77, and 46.13 N m^{-1}, respectively. $GeSnX_2$ single-layers have a very low in-plane stiffness, which is comparable with the group IV monochalcogenide single-layers.[24] Young's modulus of $GeSnX_2$ single-layers is lower than that of similar 2D structures, such as boron–carbon–nitride (291 N m^{-1}),[45] MoS_2 (130 N m^{-1}),[46] Janus group III monochalcogenides.[31] This implies that GeSnX single-layers are more flexible and could be useful for applications in nanoelectromechanical devices. Similarly, Janus $GeSnX_2$ has a high anisotropic Poisson's ratio $\vartheta(\varphi)$. The Poisson's ratio depends strongly on the investigated direction of the single-layers. It is found that, as presented in Fig. 3(b), the Poisson's ratio along the zigzag direction $\vartheta(90°)$ is the highest. Meanwhile, the Poisson's ratio along the ±45° relative to the armchair direction is the smallest.

3.3 Electronic properties

In this part, we present our calculations for the electronic properties of Janus single-layers $GeSnX_2$ (X = S, Se, Te). It is

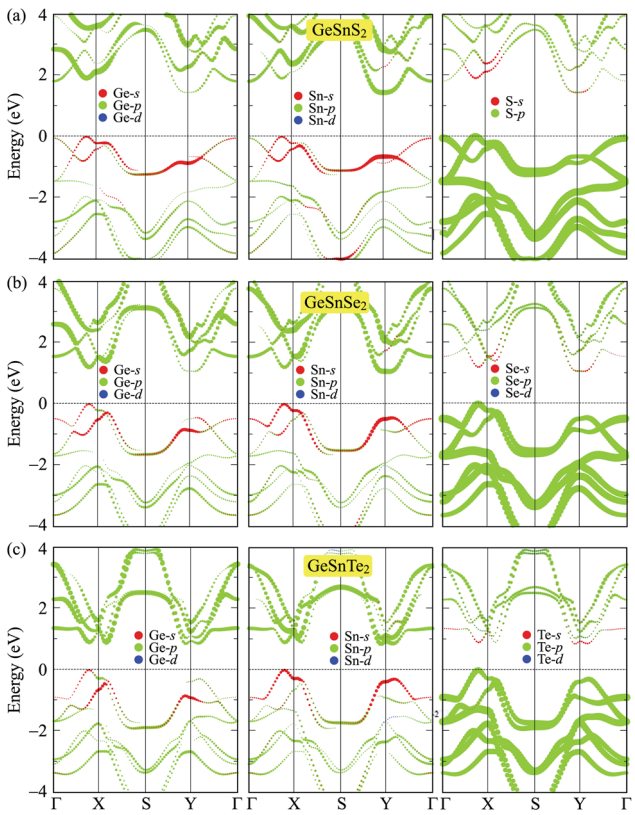

Fig. 5 Weighted bands of $GeSnS_2$ (a), $GeSnSe_2$ (b), and $GeSnTe_2$ (c) at the PBE level.

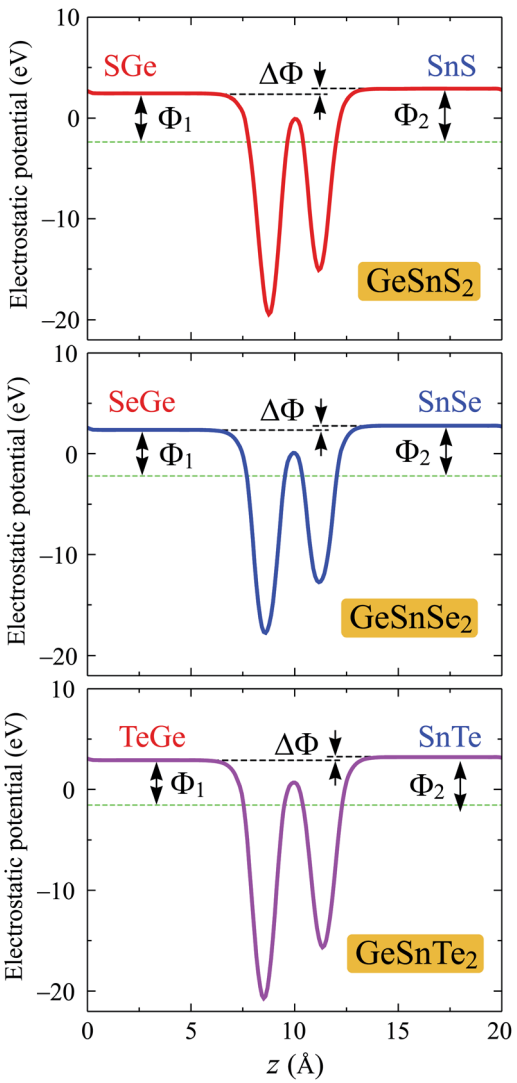

Fig. 6 Planar average electrostatic potentials of $GeSnX_2$ single-layers. $\Delta\Phi$ is the difference in vacuum level between the two sides of single-layer.

demonstrated that all three models of $GeSnX_2$ are semiconductors. The band structures of $GeSnX_2$ plotted along the Γ–X–S–Y–Γ high-symmetry direction are depicted in Fig. 4. At the PBE level, all three models of $GeSnX_2$ have an indirect bandgap with a value between 0.87 and 1.45 eV. The calculated results for the bandgap are summarized in Table 3. As shown in Fig. 4(a), the conduction band minimum (CBM) lies around the Y-point, while the valence band maximum (VBM) locates on the ΓX-path. In the case of $GeSnS_2$, the difference in energy at the VBM and Γ-point is very small, just only 0.05 eV. Meanwhile, the difference in energy at the CBM and another lowest point on the ΓX-path of the Janus $GeSnTe_2$ is even smaller (0.04 eV). It suggests that the electronic characteristics can be greatly modified when subjected to external influences such as mechanical strains or pressure. However, we know that the PBE method underestimates the energy gap precision. Therefore, we need to correct the electronic structure to achieve a more precise band gap value. The current popular and accurate method for energy structure correction is the HSE06 method. The band structures at the HSE06 level are presented in Fig. 4(b). It is found that the band diagrams evaluated by the PBE and HSE06 approaches are almost the same in profile. However, band structure correction with the HSE06 not only changes the bandgap of the single-layers but also changes the character of $GeSnTe_2$, that is, $GeSnTe_2$ has become a direct semiconductor at the HSE level despite the difference in energy between the old and new CBM positions is very small. The bandgap at the HSE06 level of $GeSnS_2$, $GeSnSe_2$, and $GeSnTe_2$ is 2.05, 1.53, and 1.33 eV, respectively.

To get more insight onto the formation of electronic bands, we calculate the weighted bands of the considered systems using the PBE method. Fig. 5 presents the calculated weighted bands of $GeSnX_2$ single-layers. In general, the projected bands of the three single-layers are quite similar. The valence band is formed by the main contribution from the p-orbitals of the X atoms, while the p-orbitals of both Ge and Sn atoms are the main contributor to the conduction band. Besides, the s-orbitals of Ge and Sn atoms contribute slightly to the valence band in the vicinity of the Fermi level. The contribution of the X-p orbitals to the conduction band is much smaller than their contribution to the valence band. It is found that VBM is contributed mainly from the p-orbitals of X atom. Ge-s and Sn-s orbitals also contribute to the formation of the VBM, however, their contribution is much smaller than that of X-s orbitals. Meanwhile, the CBM is contributed mainly from p-Ge and p-Sn orbitals and their contribution to the CBM is quite even.

One of the other important features of electrons that we examine in this section is the work function. The work function

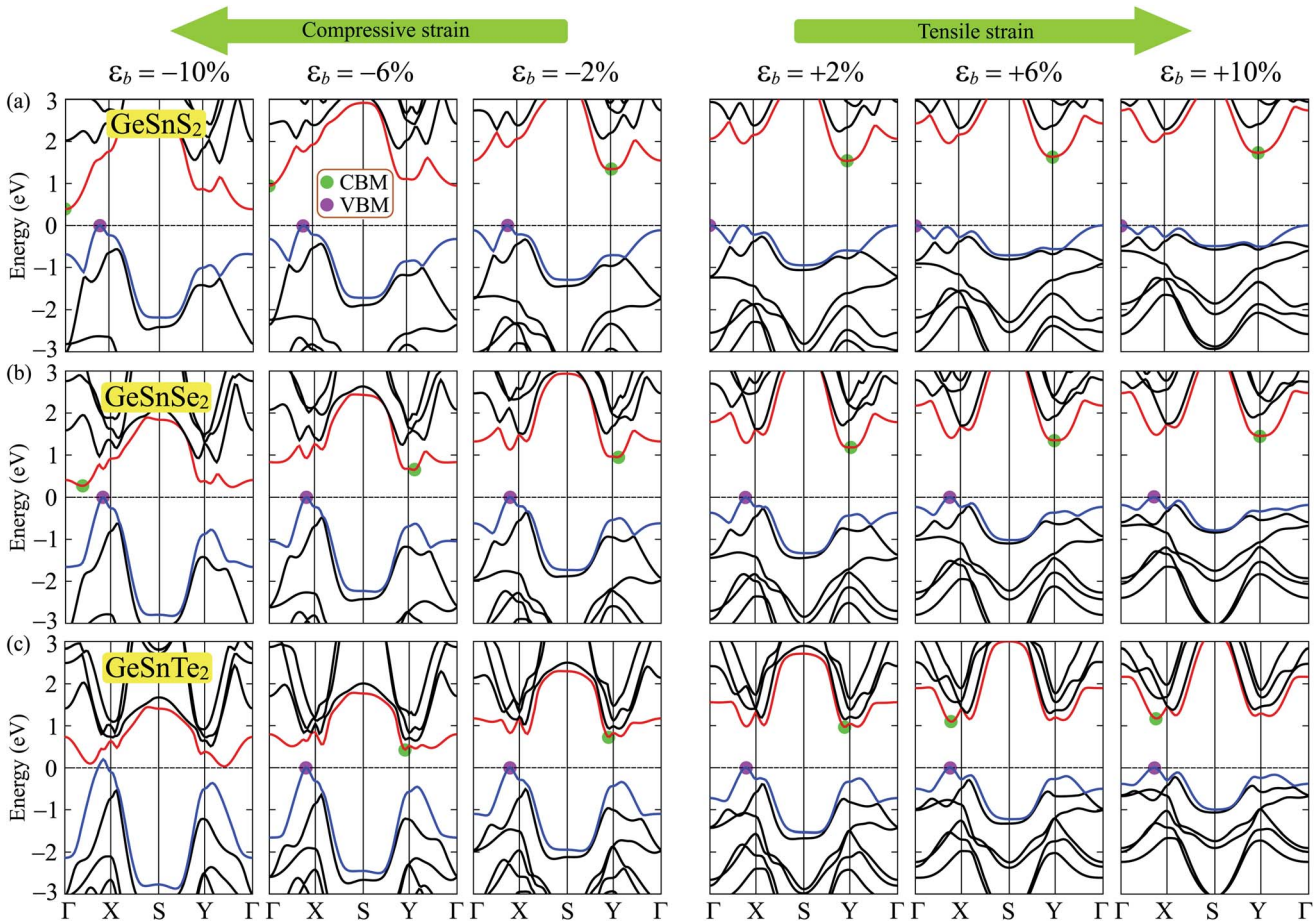

Fig. 7 Band diagrams of $GeSnS_2$ (a), $GeSnSe_2$ (b), and $GeSnTe_2$ (c) under biaxial strain with various values of ε_b.

is a physical quantity that characterizes the ability of an electron to escape from the material surfaces. The work function Φ is calculated based on the Fermi level E_F and vacuum level E_{vac} *via* the relationship $\Phi = E_{vac} - E_F$. It is noted that there exists an intrinsic built-in electric field in Janus materials due to their vertical asymmetrical structure.[35] Hence, dipole correction should be included to treat the errors caused by the periodic boundary conditions.[47] Planar average electrostatic potentials of $GeSnX_2$ single-layers are shown in Fig. 6. It is found that there is a distinct vacuum level difference $\Delta\Phi$ existing on the two different sides of asymmetry Janus single-layers, which does not exist in the 2D vertical symmetric materials such as mono-chalcogenides or dichalcogenides. This results in different work functions on the two sides of the material. The calculated results for the vacuum level difference $\Delta\Phi$ and work functions on the XGe-side Φ_1 and SnX-side Φ_2 of Janus $GeSnX_2$ single-layers are summarized in Table 3. We can see that the work function on the XGe-side Φ_1 is slightly smaller than that on the SnX-side Φ_2. It suggests that it is easier for the electron to escape from the XGe-side than from SnX-side.

Mechanical strain is one of the simplest and most efficient ways to modify the electronic states of a material. Here, we investigate the effect of biaxial strain ε_b on the electronic characteristics of $GeSnX_2$ single-layers through the PBE method. The band structures of $GeSnX_2$ single-layers under various values of the biaxial strain ε_b are depicted in Fig. 7. We can see that the band structures of the considered single-layers are strongly altered when the biaxial strain was introduced. As expected, the biaxial strain significantly changes the electronic bands near the Fermi level. As a result, there is a change in the band edge positions. From Fig. 7(a and b), we see that the CBM of $GeSnS_2$ and $GeSnSe_2$ tends to shift from the *Y*-point to the Γ point in the Brillouin region when the compressive strain is applied. Meanwhile, the tensile strain caused the CBM of the $GeSnTe_2$ to leave the *Y* point and come to lie on the ΓX path as shown in Fig. 7(c). Consequently, an indirect–direct bandgap transition is observed in $GeSnTe_2$ in the presence of tensile strain. $GeSnTe_2$ becomes direct semiconductor at $\varepsilon_b = 4\%$ with both CBM and VBM located on the ΓX path. The strain engineering not only changes the band edge positions but also drastically modulates their bandgap. Strain-dependent band gaps of Janus $GeSnX_2$ single-layers are shown in Fig. 8. It is found that while the tensile strain slightly increases the bandgap of the considered single-layers, the bandgap of all three single-layers decreases rapidly when the tensile strain is applied. Interestingly, the semiconductor–metal phase transition is found in $GeSnTe_2$ as its bandgap reduces to zero at $\varepsilon_b = -10\%$. With electronic characteristics that are easily altered by strain engineering, $GeSnTe_2$ single-layers have great prospects for applications in nanoelectromechanical devices.

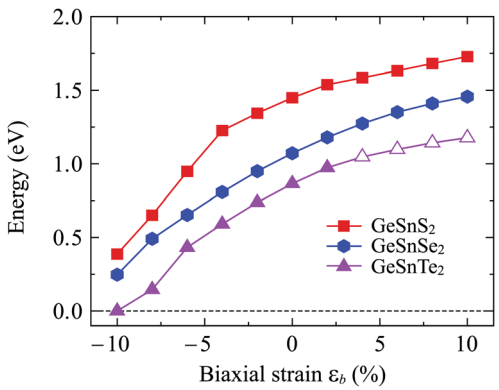

Fig. 8 Strain-dependent band gaps of Janus $GeSnX_2$ single-layers. Open and filled markers stand for the direct and indirect band gap, respectively.

4 Conclusion

In conclusion, the structural, mechanical, and electronic properties of Janus $GeSnX_2$ single-layers have been systematically investigated by the DFT calculations. The obtained results demonstrated that all three structures of $GeSnX_2$ are stable and they exhibits highly anisotropic mechanical characteristics due to their orthorhombic lattice. At the ground state, $GeSnX_2$ single-layers are semiconductors with bandgap varying from 0.87 to 1.45 eV at the PBE level and from 1.33 to 2.05 eV at the HSE06 level. More interestingly, both indirect–direct bandgap and semiconductor–metal phase transition are observed in $GeSnX_2$ when the biaxial strain is applied. With its mechanical flexibility and electronic properties easily controlled by strain engineering, $GeSnX_2$ single-layers are predicted to be materials with many promising applications in nanoelectromechanical devices.

Conflicts of interest

There are no conflicts to declare.

References

1 K. Khan, A. K. Tareen, M. Aslam, R. Wang, Y. Zhang, A. Mahmood, Z. Ouyang, H. Zhang and Z. Guo, *J. Mater. Chem. C*, 2020, **8**, 387–440.
2 N. A. Poklonski, S. A. Vyrko, A. I. Siahlo, O. N. Poklonskaya, S. V. Ratkevich, N. N. Hieu and A. A. Kocherzhenko, *Mater. Res. Express*, 2019, **6**, 042002.
3 L. Seixas, *J. Appl. Phys.*, 2020, **128**, 045115.
4 S. Barraza-Lopez, B. M. Fregoso, J. W. Villanova, S. S. Parkin and K. Chang, *Rev. Mod. Phys.*, 2021, **93**, 011001.
5 K. S. Novoselov, A. K. Geim, S. V. Morozov, D. Jiang, Y. Zhang, S. V. Dubonos, I. V. Grigorieva and A. A. Firsov, *Science*, 2004, **306**, 666.
6 B. Lalmi, H. Oughaddou, H. Enriquez, A. Kara, S. Vizzini, B. Ealet and B. Aufray, *Appl. Phys. Lett.*, 2010, **97**, 223109.
7 A. Acun, L. Zhang, P. Bampoulis, M. Farmanbar, A. van Houselt, A. N. Rudenko, M. Lingenfelder, G. Brocks, B. Poelsema, M. I. Katsnelson and H. J. W. Zandvliet, *J. Phys.: Condens. Matter*, 2015, **27**, 443002.
8 F. Feng Zhu, W. Jiong Chen, Y. Xu, C. Lei Gao, D. Dan Guan, C. Hua Liu, D. Qian, S.-C. Zhang and J. Feng Jia, *Nat. Mater.*, 2015, **14**, 1020–1025.

9 D. Kong, H. Wang, J. J. Cha, M. Pasta, K. J. Koski, J. Yao and Y. Cui, *Nano Lett.*, 2013, **13**, 1341–1347.
10 S. M. Yoon, H. J. Song and H. C. Choi, *Adv. Mater.*, 2010, **22**, 2164–2167.
11 C. Li, L. Huang, G. P. Snigdha, Y. Yu and L. Cao, *ACS Nano*, 2012, **6**, 8868–8877.
12 L. A. Burton, D. Colombara, R. D. Abellon, F. C. Grozema, L. M. Peter, T. J. Savenije, G. Dennler and A. Walsh, *Chem. Mater.*, 2013, **25**, 4908–4916.
13 T. N. Bich, S. S. Kubakaddi, L. Dinh, N. N. Hieu and H. V. Phuc, *Phys. Rev. B*, 2021, **103**, 235417.
14 K. D. Pham, N. N. Hieu, H. V. Phuc, I. A. Fedorov, C. A. Duque, B. Amin and C. V. Nguyen, *Appl. Phys. Lett.*, 2018, **113**, 171605.
15 H. T. T. Nguyen, M. M. Obeid, A. Bafekry, M. Idrees, T. V. Vu, H. V. Phuc, N. N. Hieu, L. T. Hoa, B. Amin and C. V. Nguyen, *Phys. Rev. B*, 2020, **102**, 075414.
16 P. T. Huong, D. Muoi, H. V. Phuc, C. V. Nguyen, L. T. Hoa, B. D. Hoi and N. N. Hieu, *J. Mater. Sci.*, 2020, **55**, 14848–14857.
17 C. V. Nguyen, N. N. Hieu, N. A. Poklonski, V. V. Ilyasov, L. Dinh, T. C. Phong, L. V. Tung and H. V. Phuc, *Phys. Rev. B*, 2017, **96**, 125411.
18 T. V. Vu, H. V. Phuc, S. Ahmad, V. Q. Nha, C. V. Lanh, D. P. Rai, A. I. Kartamyshev, K. D. Pham, L. C. Nhan and N. N. Hieu, *RSC Adv.*, 2021, **11**, 23280–23287.
19 T. V. Vu, H. V. Phuc, C. V. Nguyen, A. I. Kartamyshev and N. N. Hieu, *J. Phys. D: Appl. Phys.*, 2021, **54**, 475306.
20 Z. Hu, Y. Ding, X. Hu, W. Zhou, X. Yu and S. Zhang, *Nanotechnology*, 2019, **30**, 252001.
21 L. Makinistian and E. A. Albanesi, *Phys. Rev. B: Condens. Matter Mater. Phys.*, 2006, **74**, 045206.
22 L. Makinistian and E. A. Albanesi, *J. Phys.: Condens. Matter*, 2007, **19**, 186211.
23 C. Chowdhury, S. Karmakar and A. Datta, *J. Phys. Chem. C*, 2017, **121**, 7615–7624.
24 R. Fei, W. Li, J. Li and L. Yang, *Appl. Phys. Lett.*, 2015, **107**, 173104.
25 A.-Y. Lu, H. Zhu, J. Xiao, C.-P. Chuu, Y. Han, M.-H. Chiu, C.-C. Cheng, C.-W. Yang, K.-H. Wei, Y. Yang, Y. Wang, D. Sokaras, D. Nordlund, P. Yang, D. A. Muller, M.-Y. Chou, X. Zhang and L.-J. Li, *Nat. Nanotechnol.*, 2017, **12**, 744.
26 J. Zhang, S. Jia, I. Kholmanov, L. Dong, D. Er, W. Chen, H. Guo, Z. Jin, V. B. Shenoy, L. Shi and J. Lou, *ACS Nano*, 2017, **11**, 8192–8198.
27 M. J. Varjovi, M. Yagmurcukardes, F. M. Peeters and E. Durgun, *Phys. Rev. B*, 2021, **103**, 195438.
28 R. Peng, Y. Ma, S. Zhang, B. Huang and Y. Dai, *J. Phys. Chem. Lett.*, 2018, **9**, 3612.
29 T. V. Vu, C. V. Nguyen, H. V. Phuc, A. A. Lavrentyev, O. Y. Khyzhun, N. V. Hieu, M. M. Obeid, D. P. Rai, H. D. Tong and N. N. Hieu, *Phys. Rev. B*, 2021, **103**, 085422.
30 M. Demirtas, B. Ozdemir, Y. Mogulkoc and E. Durgun, *Phys. Rev. B*, 2020, **101**, 075423.
31 T. V. Vu, V. T. T. Vi, H. V. Phuc, A. I. Kartamyshev and N. N. Hieu, *Phys. Rev. B*, 2021, **104**, 115410.
32 T. V. Vu, V. T. T. Vi, H. V. Phuc, C. V. Nguyen, N. A. Poklonski, C. A. Duque, D. P. Rai, B. D. Hoi and N. N. Hieu, *J. Phys.: Condens. Matter*, 2021, **33**, 225503.
33 J. Qiu, F. Zhang, H. Li, X. Chen, B. Zhu, H. Guo, Z. Ding, J. Bao and J. Yu, *IEEE Electron Device Lett.*, 2021, **42**, 561–564.
34 P. Nandi, A. Rawat, R. Ahammed, N. Jena and A. De Sarkar, *Nanoscale*, 2021, **13**, 5460.
35 C.-F. Fu, J. Sun, Q. Luo, X. Li, W. Hu and J. Yang, *Nano Lett.*, 2018, **18**, 6312–6317.
36 P. Giannozzi, S. Baroni, N. Bonini, M. Calandra, R. Car, C. Cavazzoni, D. Ceresoli, G. L. Chiarotti, M. Cococcioni, I. Dabo, A. Dal Corso, S. de Gironcoli, S. Fabris, G. Fratesi, R. Gebauer, U. Gerstmann, C. Gougoussis, A. Kokalj, M. Lazzeri, L. Martin-Samos, N. Marzari, F. Mauri, R. Mazzarello, S. Paolini, A. Pasquarello, L. Paulatto, C. Sbraccia, S. Scandolo, G. Sclauzero, A. P. Seitsonen, A. Smogunov, P. Umari and R. M. Wentzcovitch, *J. Phys.: Condens. Matter*, 2009, **21**, 395502.
37 G. Kresse and D. Joubert, *Phys. Rev. B: Condens. Matter Mater. Phys.*, 1999, **59**, 1758.
38 J. Heyd, G. E. Scuseria and M. Ernzerhof, *J. Chem. Phys.*, 2003, **118**, 8207.
39 S. Grimme, *J. Comput. Chem.*, 2006, **27**, 1787.
40 H. J. Monkhorst and J. D. Pack, *Phys. Rev. B: Solid State*, 1976, **13**, 5188.
41 T. Sohier, M. Calandra and F. Mauri, *Phys. Rev. B*, 2017, **96**, 075448.
42 Y. Guo, S. Zhou, Y. Bai and J. Zhao, *ACS Appl. Mater. Interfaces*, 2017, **9**, 12013–12020.
43 Y. Xu, H. Zhang, H. Shao, G. Ni, J. Li, H. Lu, R. Zhang, B. Peng, Y. Zhu, H. Zhu and C. M. Soukoulis, *Phys. Rev. B*, 2017, **96**, 245421.
44 A. K. Deb and V. Kumar, *Phys. Status Solidi B*, 2016, **254**, 1600379.
45 S. Thomas and M. A. Zaeem, *Phys. Chem. Chem. Phys.*, 2020, **22**, 22066–22077.
46 R. C. Cooper, C. Lee, C. A. Marianetti, X. Wei, J. Hone and J. W. Kysar, *Phys. Rev. B: Condens. Matter Mater. Phys.*, 2013, **87**, 035423.
47 L. Bengtsson, *Phys. Rev. B: Condens. Matter Mater. Phys.*, 1999, **59**, 12301–12304.